TORSIONAL VIBRATION ANALYSIS OF SYNCHRONOUS MOTOR-DRIVEN TURBOMACHINERY

by

Mark A. Corbo

President and Chief Engineer

No Bull Engineering

Guilderland, New York

and

Clifford P. Cook

Texaco Fellow

Texaco, Inc.

Bellaire, Texas

Mark A. Corbo is the President and Chief Engineer of No Bull Engineering, a high technology engineering/consulting firm located in Guilderland, New York. He is responsible for providing rotating equipment consulting services in the forms of engineering design and analysis, troubleshooting, and third-party design audits to various clients within the turbomachinery industry. Prior to beginning his consulting career at Mechanical Technology Incorporated in 1995, he spent 12 years in the aerospace industry designing pumps, valves, and controls for gas turbine engines. His fields of expertise include rotordynamics, fluid-film journal and thrust bearings, hydraulic and pneumatic flow analysis, computational fluid dynamics, finite element analysis, dynamic simulations, and mechanical design.

Mr. Corbo has B.S. and M.S. degrees (Mechanical Engineering) from Rensselaer Polytechnic Institute. He is a registered Professional Engineer in the State of New York and a member of ASME, NSPE, STLE, and The Vibration Institute. He has authored thirteen technical publications.

Clifford P. (Cliff) Cook is with Texaco, Inc., in Bellaire, Texas. He is Chairman of the API RP 687 Task Force on Repair of Special Purpose Rotors. He is a Texaco Fellow, registered Professional Engineer in the State of Texas, Chairman of the API Subcommittee on Mechanical Equipment, and a member of the Texas A&M Turbomachinery Symposium Advisory Committee. Mr. Cook is a member of API 617 (compressors), 613 (SP gears), 677 (GP gears), 616 (gas turbines), and past member of API 684 (rotordynamics tutorial), 610 (pumps), 618 (reciprocating compressors) task forces.

Mr. Cook has a B.S. degree from the U.S. Merchant Marine Academy, Kings Point, and an M.S. degree (Mechanical Engineering) from Lehigh University.

ABSTRACT

One of the foremost concerns facing turbomachinery users today is that of torsional vibration. In contrast to lateral rotordynamics problems, torsional failures are especially heinous since the first symptom of a problem is often a broken shaft, gear tooth, or coupling. The difficulty of detecting incipient failures in the field makes the performance of a thorough torsional vibration analysis an essential component of the turbomachinery design process.

The primary objective of this paper is to provide such a procedure for the special case where the turbomachine is driven by a synchronous motor. Synchronous motors are one of the most notorious sources of torsional vibration problems because of the large pulsating torques they generate during startups. The torsional shaft stresses generated by these large pulsations are usually greater than the shaft material endurance limits, thereby causing the lives of such machines to be limited.

The determination of the number of startups that these machines can survive is, therefore, a critical portion of their design process. It is the authors' experience that there is a great deal of confusion over the proper way to do this. The full impact of this confusion was seen on a recently designed compressor train where the use of one method showed the allowable number of starts to be zero while a second procedure predicted infinite life. In an attempt to alleviate this confusion, a logical, step-by-step procedure, based on the strain-life theory of failure, was generated and is presented herein. An example illustrating how the authors used this procedure to design a critical 66,000 hp air compressor is also presented. The authors believe that employment of this method may well save the user from the need to introduce an expensive Holset-style damping coupling into some future compressor train.

INTRODUCTION

Torsional vibration is a subject that should be of concern to all turbomachinery users. By some accounts, torsional vibration is the leading cause of failures in turbomachinery drive trains. Some typical effects of uncontrolled torsional vibration are failed couplings, broken shafts, worn gears and splines, and fractured gear teeth. Accordingly, a thorough torsional vibration analysis should be included as an integral part of the turbomachinery design process. A comprehensive procedure for performing this analysis is provided in Corbo and Malanoski (1996).

The criticality of performing this analysis is heightened whenever the system is driven by an AC synchronous motor. Synchronous motors are one of the most notorious sources of torsional vibration problems because of the torque pulsations they produce during startups. Since the magnitudes of these pulsations are usually substantial, the resulting shaft stresses are often above the material endurance limits, making the shafts susceptible to fatigue. Accordingly, there is usually a definite limit to the number of startups that a synchronous motor-driven train can safely be subjected to. It is the aim of this paper to provide users with a practical analytical procedure for predicting this limit and to

highlight the criticality of proper selection of the factors employed in the analysis.

The paper begins with a brief description of synchronous motors and the mechanisms that make them such a hazard from a torsional vibration standpoint. A step-by-step procedure is then given for calculating the number of starts that a synchronous motor-driven machine can be safely subjected to. The initial steps, generation of a lumped parameter model, calculation of natural frequencies, and generation of Campbell diagrams, are only given a cursory treatment since they are described in detail in other publications. However, the later steps, performance of the time-transient analysis and, especially, determination of the shaft fatigue lives, are treated in detail.

The authors have observed that most of the existing procedures for predicting fatigue life utilize the traditional stress-life theory of failure and the traditional conservative torsional stress safety factor of 2.0. Although the predicted fatigue life and allowable number of starts are highly sensitive to both these factors (due to the log-log nature of the S-N curve), use of this method is acceptable for many machines since it errs on the conservative side.

However, the authors have, on occasion, found the traditional procedure to be too conservative. After performing a considerable amount of research, the authors have developed a more sophisticated procedure that, while still remaining conservative, provides a more accurate assessment of fatigue life. In the new procedure, the traditional stress-life theory is replaced with the strain-life theory of failure, which has consistently been found to be more accurate. Additionally, the authors found justification for using a safety factor less than the traditional 2.0 value. Furthermore, the authors implemented a rigorous method for accounting for surface finish, size, stress concentration, and notch sensitivity effects as a function of life. This is an area that the authors have observed to be a source of considerable confusion for most engineers.

The mechanics of employing the more sophisticated procedure are illustrated on a 66,000 hp air compression train and its advantages over the traditional method are clearly pointed out. The high sensitivity of the calculated number of starts to the assumed surface finish, size, stress concentration, notch sensitivity, and safety factors is also demonstrated.

SYNCHRONOUS MOTORS

AC synchronous motors are often used instead of induction motors in applications where precise speed control or higher efficiencies are desired. Unfortunately, these advantages of synchronous motors do not come without a price since, in the authors' experience, synchronous motors are the most notorious source of torsional vibration problems in turbomachinery. The primary reason for this is that synchronous motors generate large sinusoidal pulsating torques that can easily excite torsional vibrations during the startup process.

The pulsating torques occur because, unlike induction motors, synchronous motors are not self-starting. This is due to the fact that the stator's magnetic field begins rotating at synchronous speed virtually instantaneously after power is applied. With the stator rotating and the motor at rest, alternating forward and reverse torques are applied to the rotor. This causes the rotor to swing back and forth by minuscule amounts and effectively prevents the buildup of any significant accelerations in either direction.

Since synchronous motors are not self-starting, they are normally equipped with squirrel-cage (AKA amortisseur) windings, which provide starting torque and also provide damping during steady-state running. These windings are utilized to accelerate the motor as an induction motor from zero speed to a speed slightly below synchronous speed. Starting is usually performed with no voltage applied to the rotor's field winding. When synchronous speed is approached, DC field voltage is applied and the rotor is pulled into synchronism.

Pulsating torques are created during this procedure due to the fact that synchronous motor rotors contain salient poles, which are magnetic protrusions enclosed by field coils. The resulting asymmetry causes the motor's output torque to vary as a function of rotor position. This effect is in direct contrast to pure induction motors that have symmetric rotors and a generated torque that is independent of rotor location.

Synchronous motors are often modeled as having two axes of symmetry, the direct axis and the quadrature axis. The direct axis refers to a centerline that passes directly through one of the rotor's salient poles. When the direct axis is in perfect alignment with the magnetic field established by the stator, the magnetic reluctance between rotor and stator reaches a minimum value. Accordingly, the torque produced in this position, known as the direct axis torque, represents an extreme (maximum or minimum) value produced during a revolution of the rotor.

On the other hand, the quadrature axis is a centerline that is perpendicular to the direct axis. The condition where this axis is aligned with the stator's magnetic field represents the point of maximum magnetic reluctance. The resulting torque, which is referred to as the quadrature axis torque, represents the opposite extreme from the direct axis torque.

Accordingly, as the rotor rotates, the torque varies in a roughly sinusoidal fashion between the limits imposed by the direct axis and quadrature axis torques. The mean value of these two is referred to as the average torque and represents the torque available to provide acceleration to the system's inertias. Superimposed on this torque is a pulsating torque whose magnitude is one-half the difference between the direct and quadrature axis torques. Figure 1 illustrates the various torque components as a function of speed for a hypothetical synchronous motor.

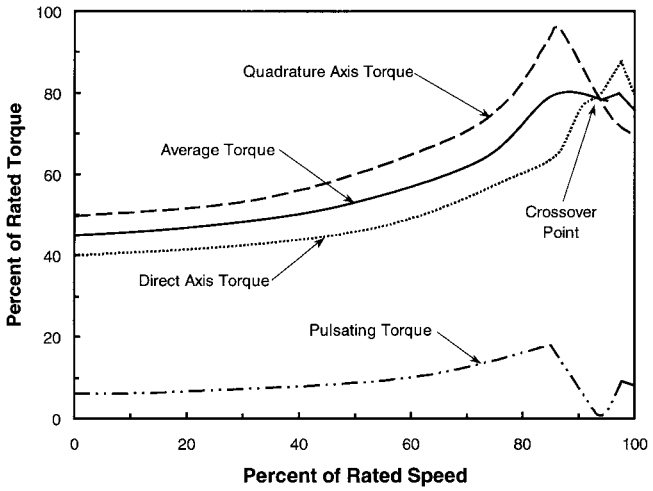

Figure 1. Typical Synchronous Motor Torque-Speed Curve.

The frequency of the torque pulsations is the frequency at which the stator's rotating magnetic field passes a rotor pole. Since the stator's magnetic field rotates at synchronous speed, the excitation frequency is a function of the difference between synchronous speed and rotor speed, which is known as slip speed. Specifically, excitations occur at twice slip frequency where slip frequency is defined by the following equation:

$$f_{slip} = f_l \bullet (N_s - N) / N_s \quad (1)$$

where:
f_{slip} = Slip frequency (Hz)
f_l = Line frequency (Hz)
N_s = Synchronous speed (rpm)
N = Rotor speed (rpm)

The motor's synchronous speed is given by the following equation:

$$N_s = 120 \bullet f_l / N_p \quad (2)$$

where:
N_s = Synchronous speed (rpm)
f_l = Line frequency (Hz)
N_p = Number of poles in motor

The ramifications of Equation (1) are extremely important. It is seen that the frequency of torque pulsations, twice slip frequency, decreases as rotor speed increases. Thus, at zero speed, the excitation frequency is equal to two times line frequency or 120 Hz in the United States. As the motor is accelerated, the excitation frequency decreases linearly until it reaches zero when the motor achieves synchronous speed.

The impact that this behavior has on the torsional vibration response of the machine is best illustrated by the Campbell diagram for a hypothetical system presented in Figure 2. In a Campbell diagram, all the unit's torsional natural frequencies are plotted as horizontal lines and the operating (synchronous) speed is denoted by a vertical line. The synchronous motor excitation line is then generated by connecting the point corresponding to twice line frequency (120 Hz) on the y-axis with the point corresponding to synchronous speed (1800 rpm) on the x-axis. Any intersection points between the excitation line and the natural frequency lines (there are three in the figure) are known as interference points. These represent potential resonances that can be triggered during startup.

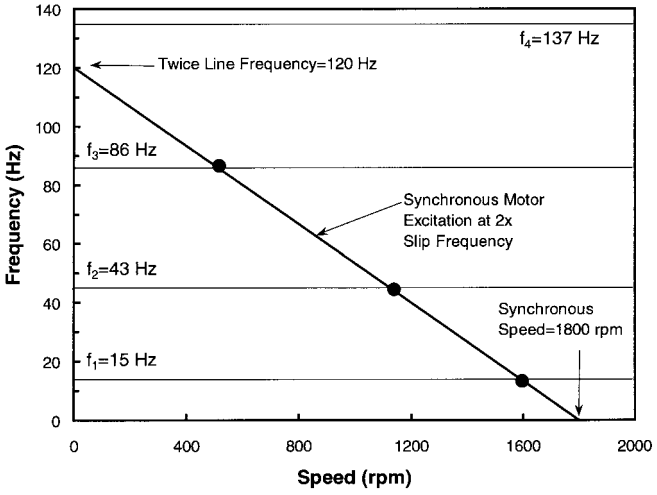

Figure 2. Typical Synchronous Motor Campbell Diagram.

It is easily seen from the figure that the motor generates interferences with all natural frequencies that are below twice line frequency. This situation is, by no means, unique to the example selected. In fact, all systems driven by synchronous motors will contain interferences with all natural frequencies below twice line frequency that could be excited during starting. This is a significant source of potential problems since most practical turbomachinery drive trains have several natural frequencies within this range.

UNDAMPED ANALYSIS

From the preceding discussion, it is easily seen that all turbomachinery drive trains driven by synchronous motors must be subjected to a rigorous torsional vibration analysis during the design phase of the program to assure structural adequacy. It is, therefore, the primary intent of this paper to present such a procedure.

Under normal circumstances, the torsional analysis should be performed within 10 weeks of order placement to allow shaft sizes and geometries to be modified without affecting delivery. In addition, it should be provided to each of the individual component vendors to obtain their concurrence. Unfortunately, this analysis is typically among the last analyses to be performed during the design phase so that changes resulting from its performance often impact equipment delivery schedules, sometimes dramatically. The authors cannot overemphasize the perils involved in following this typical path.

The first step in the analysis procedure is the generation of a lumped parameter model such as the simplified one shown in Figure 3. The model consists of a series of interconnected disk and shaft elements. The disks represent the machine's significant inertial components while the shafts behave as torsional springs. Detailed guidelines for generating such a model from hardware drawings are provided in Corbo and Malanoski (1996).

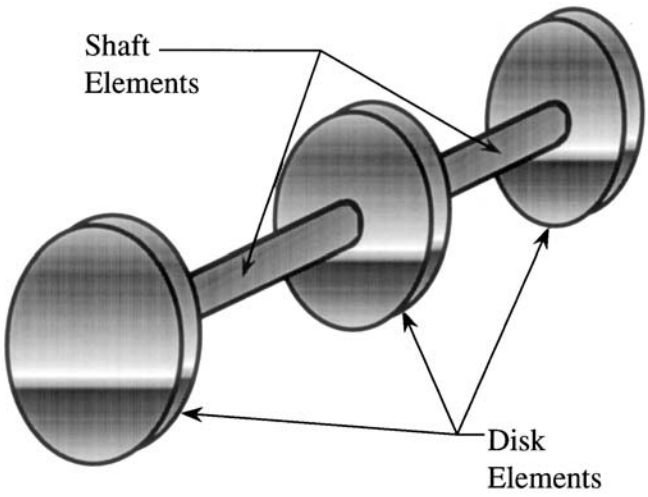

Figure 3. Sample Lumped Parameter Model.

Once the model is completed, the system's undamped natural frequencies should be calculated. Since there is a plethora of computer codes available for performing this computation, no further elaboration is required. Once the computer results are obtained, the authors recommend performing a quick "sanity check" using hand analysis to validate the computer analysis. Several quick methods for doing this are provided in Corbo and Malanoski (1996).

Once the undamped analysis has been validated, a Campbell diagram, similar to that of Figure 2, should be generated. The Campbell diagram allows the determination of the system's potential resonance points and provides an excellent overview of the machine's torsional vibration behavior, analogous to the role played by the critical speed map in a lateral rotordynamics study. For the sake of simplicity, this discussion will focus solely on the excitation generated during the synchronous motor startup. Naturally, in all real systems, there are other excitations present that also must be included in the Campbell diagram.

Once the Campbell diagram has been generated, it should be checked for interference points. In the highly unlikely scenario that there are no such points present, the analysis is finished and the system can be sanctioned. However, the much more probable situation is that there are several such points. In this case, the impact of passing through those resonance points must be evaluated via a transient response analysis of the startup.

TRANSIENT RESPONSE ANALYSIS

In the transient response analysis, the synchronous motor's excitations are applied to the system and the resulting vibratory torques and stresses are computed for each shaft element. Damping due to various sources is included in the model. The induced

torques and stresses are then compared to allowable values to determine if the system is structurally adequate.

As was previously stated for undamped natural frequency analysis, there are a number of computer codes available for the transient analysis of torsional systems. The large majority of them use numerical, time-stepping procedures. In these, the differential equations of motion for the lumped model's disks are integrated numerically using methods such as Runge-Kutta and the Newmark-β method. The analysis begins at time zero with all parameters set to their initial values. The numerical approximations, which define a parameter's new value in terms of its previous value, are then used to determine all parameter values after the first time increment. This procedure is continued in a time-marching manner until the machine reaches synchronous speed. This procedure, therefore, estimates the time history of all relevant parameters in the system. Chen (1995), Evans, et al. (1985), and Szenasi and von Nimitz (1978) all discuss numerical integration methods in much greater detail.

In using algorithms employing the Runge-Kutta numerical integration procedure, the one with which the authors are most familiar, the selection of the time step is critical from the standpoint of solution stability. Per the authors' experience, the time step must be made less than approximately one-fifth of the period corresponding to the machine's highest natural frequency. Since a torsional model has as many degrees of freedom (and natural frequencies) as the number of shaft elements in the model, the highest natural frequency for a typical turbomachinery drive train, whose model often contains more than 50 shaft elements, can be astronomically high. Accordingly, if such a model were to be subjected to a time-transient analysis using the Runge-Kutta method, the required time step would be so infinitesimally small that the analysis would be totally impractical.

The authors normally solve this problem by reducing the lumped parameter model to a much smaller model, usually consisting of about five disk elements. Since such a model has only four natural frequencies, reasonable time steps can be employed when working with it. Reduction in model size carries a couple of other benefits, as well. First of all, the amount of data generated in the transient analysis of a five-disk model, although still substantial, is much more manageable than that generated when using a much larger model. Secondly, since time-marching analyses require a substantial amount of computer time, the reduction in model size makes the computer time more reasonable. This consideration, a huge one just a few years ago, has lessened in significance with the advent of modern high-speed computers. An example case where an initial model containing 130 stations is reduced to one having only seven is provided by Bogacz, et al. (1990).

The reason that a large multidisk model can be replaced by a much simpler five-disk one without much sacrifice in accuracy is that, in the large majority of practical cases, the only natural frequencies that participate significantly in the synchronous motor startup are the first two (and the second mode's participation is often minor). In fact, Sohre (1965), Pollard (1980), and Wright (1975) all state that most synchronous motor resonance problems involve only the first (also known as the fundamental) mode. Thus, as long as the simplified model's first two natural frequencies, particularly the first, are reasonably close to those of the original model, the accuracy of the analysis is preserved.

Two basic principles are utilized in the conversion of multidisk models to five-disk ones. The first is that relatively small inertias have very little effect on the machine's first two natural frequencies. These disks can, therefore, be ignored and the shaft elements on either side of them can be combined as springs in series. The second principle is that shafts having relatively large torsional stiffnesses behave as if they were rigid in the first two modes. Accordingly, these elements can be discarded and the inertias on either side of them can be simply added together.

Although some judgment must be exercised in deciding where to place the five disks, some general rules can be stated. The large majority of applications involving synchronous motors that the authors are familiar with involve the motor driving a compressor through a speed-increasing gearbox. In such cases, the authors generally locate one disk at the motor's rotor, one at the gear mesh, and one at the compressor's main wheel. The other two are usually located in the vicinity of the two couplings, one on each side of the gear mesh.

Since some of the transient response programs that the authors have seen do not have the capability of handling multiple shafts rotating at different speeds, it is often necessary to make the five-disk model an "equivalent model" that runs at the motor shaft speed. This model has exactly the same dynamic characteristics and natural frequencies as the actual system. To generate the equivalent model, the parameter values for all elements on the motor shaft are left unchanged. However, all elements on the compressor shaft must be transformed via the following equations:

$$J_{eq} = J \bullet N^2 \tag{3}$$

$$k_{eq} = k \bullet N^2 \tag{4}$$

where:
J_{eq} = Equivalent inertia referenced to motor shaft
J = Actual inertia
N = Gear ratio (ratio of compressor speed to motor speed)
k_{eq} = Equivalent stiffness referenced to motor shaft
k = Actual stiffness

Since the equivalent inertia referred to the motor shaft is equal to the product of the actual inertia and the square of the gear ratio, there is usually a significant difference between the equivalent and actual values. It is, therefore, crucial that the compressor inertia data used for sizing the motor be clearly labeled with regard to the speed that it is relative to.

Once the five-disk model is obtained, an undamped analysis should be run to ensure that its first two natural frequencies have not deviated significantly from those of the original model. If some deviation is observed, the five-disk model should be tweaked to reduce the discrepancies to acceptable levels.

Once the model to be used for the transient analysis is complete, the next step is to specify the machine's performance and damping characteristics. The performance characteristics that are needed include the motor's average and pulsating torque and the compressor's load torque as a function of speed over the entire speed range from standstill to synchronous speed. The need for the pulsating torque is obvious since it represents the excitation being applied to the system. However, the motor's average and compressor's load torques are also important since they determine the machine's acceleration rate.

During startups, the net torque available to accelerate the machine is equal to the motor's average torque minus the load torque. The system acceleration rate in the vicinity of the resonant speed is crucial because it determines the length of time (dwell time) that the machine spends at resonance. The longer the dwell time, the more likely the machine is to experience problems, for two reasons. First, longer dwell times introduce a larger number of damaging high-stress cycles. Second, longer dwell times mean larger torque peaks since they give the response more time to build up toward the steady-state value (which corresponds to an infinite dwell time). Accordingly, designers should aim to maximize the system's acceleration rate in the vicinity of the fundamental mode's resonant speed.

The motor torque should be based on the voltage at the motor terminals, not line voltage. A conservative approach is to not account for any voltage recovery as the train increases in speed. The compressor torque is generally based on throttling the compressor suction to reduce the required horsepower. Care must be taken for refrigeration systems since the compressor suction

pressure may settle out at a much higher pressure than under normal operation.

Damping must also be applied to the system in order to limit the response at resonance (which is theoretically infinite for the undamped case) to finite values. The damping due to localized sources can be calculated using the methods given in Corbo and Malanoski (1996) and applied to the appropriate elements. However, the authors have found this to be a time-consuming and often unnecessary step.

Instead, the authors advocate accounting for damping by merely applying a generic damping ratio to each shaft element in the model. This generic ratio accounts for effects, such as hysteretic and slip damping, that are present in all real systems but are extremely difficult to quantify.

A search of the literature revealed some difference in opinion on the magnitude of the damping factor that should be applied. Chen, et al. (1983), cite a typical range of three to five percent of the critical value for geared systems. Anwar and Colsher (1979) are in basic agreement, giving a range of two to five percent. Mruk, et al. (1978), give exactly the same range. Wright (1975) recommends the use of a factor of 1.25 percent for ungeared systems and 2.0 percent for geared machines.

The reason why geared systems are distinguished from ungeared ones is that geared systems generally contain more damping. There are two primary reasons for this. The first is that most turbomachinery gearshafts are supported on fluid-film journal bearings. Although the viscous friction that is inherent in these bearings provides very little damping, if there is any lateral motion accompanying the torsional vibration, the fluid in the bearing's radial clearance is forced to flow circumferentially, thereby generating a squeeze-film effect. Simmons and Smalley (1984), Draminsky (1948), and Shannon (1935) all describe torsional systems in which this was the predominant source of damping in the system. Of course, the torsional-lateral coupling necessary to generate this phenomenon is present only in geared machines.

The second is that, in synchronous motor startups, the cyclic torques occurring at gear meshes at resonance are normally greater than the transmitted torque. In this situation, known as a torque reversal, the resulting negative net torque causes the gear drive surfaces to separate and the teeth to move through their backlash until they make contact on their nondrive surfaces. Once the torque becomes positive again, the teeth are driven back through their backlash until they resume contact on their original surfaces. This results in successive impacts of the gear teeth that dissipate energy via generation of shock waves and eddies. This so-called impactive damping increases the overall system damping.

Thus, the one conclusion that can be drawn from the various references is that the minimum amount of damping that can be expected for a typical geared machine consisting of a motor, gearbox, and compressor is two percent of the critical value. Since the authors have found this value to be conservative for such machines, this is the value recommended for use in the absence of actual test data.

Some care should be taken when applying this generic damping ratio since the authors are aware of common misinterpretations that yield incorrect damping coefficients for the individual shaft elements. The damping coefficients for each shaft element, which will all be different, should be calculated using the following:

$$C_n = 2 \bullet \Gamma \bullet k_n / \omega_n \quad (5)$$

where:
C_n = Damping coefficient for nth shaft (lbf-sec/in)
Γ = Damping ratio
k_n = Stiffness of nth shaft (lbf/in)
ω_n = First torsional natural frequency (rad/sec)

Since torque reversals are commonly encountered, another characteristic of geared machines that is sometimes accounted for in the transient analysis is the backlash between the gear teeth. Including this tends to reduce the predicted peak torques at resonance since the motor's excitation torques are not applied to the compressor shaft during torque reversals. However, Chen, et al. (1983), and the authors have found that the impact of including this effect is usually minor and, thus, recommend conservatively ignoring it.

Once the transient model is completed, the time-transient analysis program should be run to obtain the torque versus time history for each relevant shaft element in the model. A typical plot will look like Figure 4 where the torque cycles at a fairly steady level until resonance with the fundamental natural frequency is approached. At this point, the torque magnitudes begin increasing until they reach a peak at the resonance point. After this, the torque magnitudes begin to decrease until the resonance zone is exited, after which the torques remain fairly constant at a relatively low level.

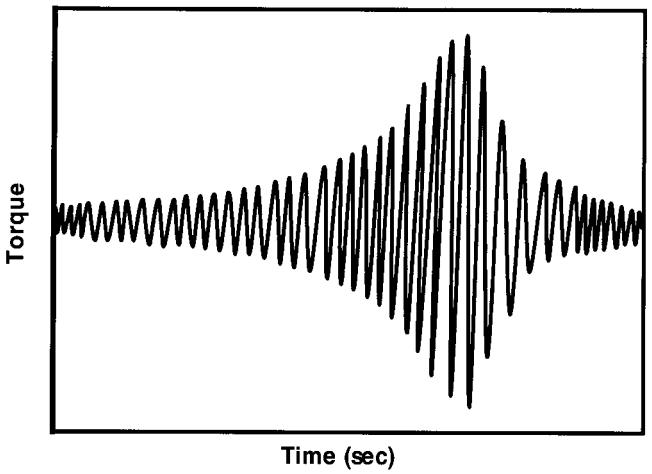

Figure 4. Typical Synchronous Motor Response.

DETERMINATION OF SHAFT FATIGUE LIVES

Once the torque versus time history for a shaft element is known, the life of the shaft can then be calculated. The first step in life determination is the identification of the maximum and minimum torque values for each cycle within the resonance zone. There are a number of ways to convert the results of a transient analysis, which are typically in the form of Figure 4, into a list of cycles having minimum and maximum torques. For the sake of clarity, the descriptions of these methods along with the authors' recommendations will be held off until the example problem is discussed.

The next step is identification of the region or regions within the shaft element that constitute the "weak links" and are most likely to fail. These regions almost always contain geometric stress risers such as steps in shaft diameter and are usually located at relatively small diameters. The one exception to this occurs when the shaft contains a keyway. Since the stress concentration factors arising at keyways are normally very high, regions containing keyways should always be checked out even if they are at large diameters. For the regions of interest, the maximum and minimum torques should be converted to maximum and minimum shear stress values using the following equation from strength of materials:

$$\tau = T \bullet R / I_p \quad (6)$$

where:
τ = Shear stress (psi)
T = Torque (in-lbf)
R = Shaft outside radius (inch)
I_p = Shaft area polar moment of inertia (in^4)

The maximum and minimum shear stresses so obtained should then be combined to obtain the cyclic stresses occurring in each torque cycle. It should be noted that in fatigue problems such as this where the mean stress is non-zero, it is technically necessary to calculate both the mean and cyclic stresses in order to determine life. However, Evans, et al. (1985), Walker, et al. (1981), and the authors have found that in synchronous motor startups, the magnitude of the mean stress is so much lower than that of the cyclic stress that the mean stress can be safely ignored. Thus, only the cyclic stress needs to be calculated, using the following equation:

$$\tau_{cyclic} = 0.5 \bullet (\tau_{max} - \tau_{min}) \tag{7}$$

where:
τ_{max} = Maximum stress
τ_{min} = Minimum stress
τ_{cyclic} = Cyclic stress

Determination of the cyclic stress is the easy part of the life prediction procedure. The part that confuses many engineers is the determination of the allowable stress that this cyclic stress should be compared to. Although the authors do not pretend the procedure that follows is the only legitimate one that can be used for this, they do believe it is more accurate than the large majority of methods currently being used.

Strain-Life Theory of Failure

The primary difference between the advocated procedure and most other procedures currently being used is that it relies on the strain-life theory of failure rather than the traditional S-N curve (stress-life theory). When the traditional S-N curve is employed, it is implicitly assumed that the life of a part is directly dependent on the level of stress it carries. On the other hand, the strain-life theory is based on the empirical finding that the parameter that determines the life of a part is strain (i.e., displacement), not stress (i.e., load).

In the traditional stress-life method, stress is plotted versus number of cycles on log-log paper. Shigley and Mischke (1989) speak for many authors when they advocate the following simple method for generating the S-N curve. In the absence of more precise test data, the tensile endurance limit can be approximated as being equal to one-half of the material's ultimate tensile strength and should be taken to correspond to a life of 10^6 cycles. In the low cycle fatigue regime, the strength at a life of 10^3 cycles should be set equal to 90 percent of the ultimate tensile strength. The complete S-N curve can then be generated by connecting these two points by a straight line on a log-log plot of stress versus life.

Shigley and Mischke (1989) point out that the S-N curve generated via the above procedure has the following governing equations:

$$S(N) = a \bullet N^b \tag{8}$$

$$a = (.90 \bullet UTS)^2 / Se \tag{9}$$

$$b = -1/3 \bullet \log(.90 \bullet UTS / Se) \tag{10}$$

where:
N = Number of fully-reversing cycles
S(N) = Cyclic stress corresponding to a life of N cycles (psi)
UTS = Ultimate tensile strength (psi)
Se = Tensile endurance limit (psi)
a, b = Empirical constants

The use of the S-N curve is quite simple. For a given fully-reversing stress level, the above equations or the plot can be used to find the life corresponding to that stress.

Although the traditional stress-life method is a perfectly acceptable procedure for evaluating the fatigue lives of shafts, it tends to be conservative due to the following two effects:

- Most experts agree that the endurance limit corresponds to a life somewhere between 10^6 and 10^7 cycles. Accordingly, assuming that the life corresponding to the endurance limit strength is only 10^6 cycles is conservative.

- Shigley and Mischke (1989) state that in order for a fatigue failure to occur, cyclic plastic deformations must be present. Boyer (1986) concurs, stating that fatigue failures are the product of the simultaneous action of cyclic stresses, tensile stress, and plastic strain. Since the presence of plastic strain is needed for a fatigue failure to occur, the life of a part is a function of both its strength and its ductility. Since the stress-life method does not account for ductility effects, it tends to under-predict the lives of parts made from ductile materials.

The strain-life theory deviates from this by assuming that the life of a part is dependent on the level of strain, not stress, occurring in the part. Shigley and Mischke (1989) speak for most experts in the field when they claim that the strain-life theory is the best existing theory for predicting fatigue failures. This is consistent with the authors' experience that the stress-life method, while being perfectly valid, tends to be conservative. On the other hand, the strain-life theory, while still erring on the conservative side, is a much more accurate predictor of shaft life.

The basis of the strain-life theory is that the relationship between applied strain and life is as illustrated in Figure 5, taken from Shigley and Mischke (1989). It is seen from the figure that the total strain in a part is the sum of the elastic strain and the plastic strain. It is also seen that both the elastic and plastic strains are linearly related to part life when plotted on log-log paper. For this reason, this theory is also commonly referred to as the universal slopes theory. It is further seen that, in the high cycle fatigue (HCF) regime, that the total strain is primarily elastic strain. On the other hand, in the low cycle fatigue (LCF) region, the plastic strain predominates.

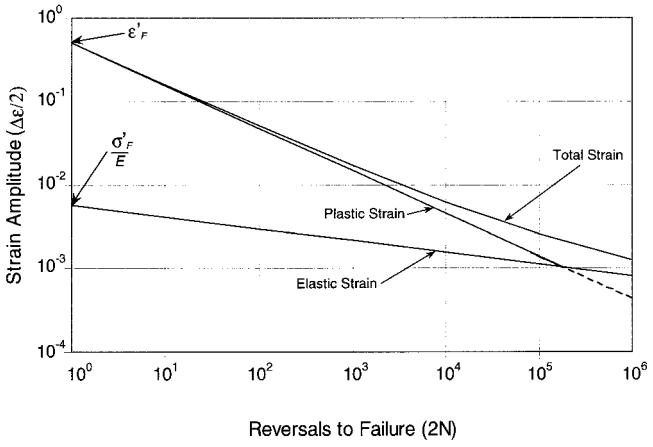

Figure 5. Typical Strain Versus Life Curve.

Boyer (1986) points out that most people arbitrarily set the dividing line between low and high cycle fatigue somewhere between 10^4 and 10^5 cycles. However, a more accurate dividing criterion is whether the predominant component of strain imposed during cyclic loading is elastic or plastic. In fact, Mischke (1982) defines the dividing line between LCF and HCF as the point where the elastic and plastic strains are equal.

The baseline equation for the strain-life theory is the Coffin-Manson equation, which assumes that the total strain versus life curve behaves in the manner of Figure 5:

$$\varepsilon(N) = (\sigma_f` / E) \bullet N^b + \varepsilon_f` \bullet N^c \tag{11}$$

where:
N = Life (cycles)
$\varepsilon(N)$ = True strain corresponding to a life of N cycles
σ_f' = True stress at fracture during tensile test (psi)
ε_f' = True strain at fracture during tensile test
b = Elastic strain exponent (slope of elastic strain line)
c = Plastic strain exponent (slope of plastic strain line)
E = Elastic modulus (psi)

Equation (11) is the equation that the authors advocate using for determining the strain versus life behavior of a given shaft subjected to torsional vibration. The elastic and plastic strain exponents are material characteristics that can be obtained from Boyer (1986), Shigley and Mischke (1989), or any other resource containing material fatigue properties. The true stress and true strain at failure can be directly obtained from the tensile test results per the following:

$$\sigma_f' = UTS/(1-RA) \tag{12}$$

$$\varepsilon_f' = \ln(1/(1-RA)) \tag{13}$$

where:
UTS = Ultimate tensile strength (psi)
RA = Reduction in area

It is seen that whereas the stress-life method did not take the material's ductility into account, the strain-life method accounts for the material's reduction in area, a direct measure of ductility.

Equation (11) gives the strain versus life characteristics for any shaft element of interest. However, unless a finite element code is employed during the transient startup analysis, the strains imposed on the shafts are usually unknown. Instead, the known parameter for each shaft element is stress. The logical question is then how the relation of Equation (11) can be converted into an equation, similar to Equation (8), relating stress and life.

In an attempt to answer this question, the authors consulted with a number of fatigue experts of their acquaintance. The consensus of these experts was that the strain-life curve should be converted into a stress-life curve by merely multiplying the strains by the material's elastic modulus, *E*. This is not purely correct since the assumption that the stress is equal to the product of the strain and the elastic modulus is only valid for elastic strains. As is shown by Mischke (1982), the relationship between plastic stresses and strains is much more complex.

However, the experts justified their recommendation by noting that for the large majority of synchronous motor startup calculations, the portion of the curve that is of interest is the portion where the elastic strain is greater than the plastic strain. This is because the proposed version of API 617 indicates that compressors being driven by synchronous motors are generally capable of surviving at least 1500 starts. Thus, using Miner's cumulative damage rule, which will be described in detail later, with a limiting summation value of 0.5 and assuming 10 torsional cycles per start, the smallest number of allowable cycles will be 30,000 (1500 • 10 / 0.5). In fact, in the example provided later to illustrate the authors' procedure, the smallest number of allowable cycles is 61,600, which lies in the HCF region of the strain versus life curve for most engineering materials. Accordingly, the error introduced by making an approximate conversion of plastic strain to stress is small.

In order to test the validity of this recommendation, the authors used the recommended procedure on a 4340 steel shaft and compared its results with those obtained using the much more complicated procedure given by Mischke (1982). As expected, the allowable stress at a life of 1000 cycles predicted by the recommended procedure was about three times that predicted by the more sophisticated method. However, at a life of 10,000 cycles, the recommended procedure over-predicts the strength by about 35 percent and at a life of 30,000 cycles, it is only 7.5 percent high. At lives above 40,000 cycles, there is virtually no difference between the two methods. Accordingly, it is concluded that merely multiplying the strains of Equation (11) by the elastic modulus to obtain stresses is perfectly valid for the large majority of synchronous motor startup problems that the user is likely to encounter. However, the user should always remember the limitations of this method when dealing with small numbers of cycles.

Strength Derating Factors

Multiplication of Equation (11) by the elastic modulus yields the baseline tensile stress versus life curve for the shaft material of interest. This curve must then be multiplied by a number of factors to obtain the shear stress versus life curve for the actual shaft element, as follows:

$$\tau(N) = S(N) \bullet Fsh \bullet ka \bullet kb / (kf \bullet SF) \tag{14}$$

where:
$\tau(N)$ = Allowable shear stress for a life of N cycles (psi)
N = Number of fully-reversing cycles
S(N) = Allowable tensile stress for a life of N cycles (psi)
Fsh = Shear factor
ka = Surface finish factor
kb = Size factor
kf = Fatigue stress concentration factor
SF = Safety factor

In the authors' experience, determination of the derating factors in Equation (14) is one of the most confusing and misunderstood aspects of analyzing synchronous motor startups. For that reason, the proper method for determining each of these factors will be discussed in detail.

Shear Factor

The shear factor, *Fsh*, is included to reflect that a material's strength in shear is less than its tensile strength. This factor is merely the ratio of a material's shear strength to its tensile strength for the same number of applied cycles. There are two major failure theories, both discussed in Shigley and Mischke (1989), for determining this factor. The more conservative theory is the maximum shear stress theory that predicts this ratio is 0.50. The second theory is the distortion energy (AKA von Mises) theory that gives this ratio as 0.577.

The authors are acquainted with some engineers, such as Szenasi and von Nimitz (1978), who believe that the maximum shear stress theory should be used for synchronous motor startups because it is more conservative. However, it is the authors' experience that the distortion energy theory is a more accurate predictor of the actual shaft strength. This viewpoint is shared by Banantine, et al. (1990), Juvinall (1967), and Shigley and Mischke (1989). Accordingly, the authors advocate the use of the distortion energy theory and a shear factor of 0.577.

Surface Finish Factor

The surface finish factor, *ka*, accounts for the fact that the susceptibility of a part to fatigue failures can be drastically reduced by improving its surface finish. This is because the scratches, pits, and machining marks, which are more prevalent in a rough surface, add stress concentrations to the ones already present due to part geometry. Since most published material properties are obtained from tests performed on finely polished specimens, the fatigue strengths of most parts will be less than the published values. The surface finish factor represents the ratio of the part's fatigue strength to that of the test specimen, based on surface finish considerations.

Shigley and Mischke (1989) provide the following equation for calculating the surface finish factor:

$$ka = a \bullet UTS^b \tag{15}$$

where:
ka = Surface finish factor
UTS = Ultimate tensile strength (ksi)
a, b = Empirical coefficients dependent on manufacturing method

Coefficients *a* and *b* are given in Table 7-4 of Shigley and Mischke (1989) for various surface finishing processes. For machined surfaces, *a* is equal to 2.70 and *b* equals −0.265. Although it is not explicitly listed in the table, the surface finish factor for a polished surface is 1.0.

Most of the engineers of the authors' acquaintance account for surface finish effects by utilizing the above factor to derate the strength at all lives on the S-N curve. The authors feel that this is over-conservative since Boyer (1986) points out that the surface finish factor calculated using the above equation only applies to the endurance limit at 10^6 cycles. At all other lives, the effect of surface finish is reduced until a life of 1000 cycles is reached, where it has no effect whatsoever (ka = 1.0).

Although Boyer (1986) does not give any methodology for determining the surface finish factor at lives between 1000 and 10^6 cycles, using the same arguments that are provided later for the size and stress concentration factors, the authors have assumed that the relationship between surface finish factor and life is linear when plotted on log-log coordinates. Utilizing that assumption, the relevant equations for surface finish factor as a function of life can be shown to be as follows:

$$ka(N) = 10^b / N^m \tag{16}$$

$$m = \log[ka(1000)/ka(10^6)]/3.0 \tag{17}$$

$$b = \log\{[ka(1000)]^2/ka(10^6)\} \tag{18}$$

where:
ka(N) = Surface finish factor for a life of N cycles
ka(10^6) = Surface finish factor for 10^6 cycles (from Equation (15))
ka(1000) = Surface finish factor for 1000 cycles (1.00)
m = Slope of ka versus N line on log-log coordinates
b = Intercept of ka versus N line on log-log coordinates

Thus, it is seen that the surface finish factor varies from a maximum value of 1.0 at 1000 cycles to a minimum value of that given by Equation (15) at 10^6 cycles.

Size Factor

The size factor accounts for the empirical observation that when two shafts are manufactured from the same batch of material and tested at the same level of surface strain, the larger diameter shaft will almost always fail in a lower number of cycles than the other shaft. There are three general theories for why this size effect exists. The first recognizes that fatigue failures almost always initiate at the location of a flaw in the material. Since a shaft containing a larger volume of material is statistically more likely to contain such a flaw, the susceptibility of a shaft to fatigue failure increases with shaft diameter.

The second theory is very similar to the first except that it is based on surface area instead of volume. This theory states that since almost all fatigue failures initiate at a flaw on the surface of a part, larger parts are more vulnerable since they have larger surface areas and are, thereby, more likely to contain surface flaws.

The third theory, as espoused by Banantine, et al. (1990), is based on the assumption that the susceptibility of a part to fatigue failure is directly dependent on the volume of the thin layer of surface material that is subjected to a stress level within 95 percent of the stress at the surface. Since a larger component will have a shallower stress gradient than a smaller part, the larger part will have a larger volume subjected to this high stress. This makes the larger part more vulnerable to fatigue failures. Empirical results that reveal that size effects are much less important for axial loadings, where there is no stress gradient, than for bending or torsional loadings provide backing for this hypothesis.

Regardless of what mechanism is at work, there is no question that larger shafts subjected to torsional loadings will fail in less cycles than smaller shafts. Additionally, since most shafts used in practical turbomachines are larger than the 0.25 to 0.30 inch diameter shafts usually used to generate published strength data, the size effect almost always involves a reduction in strength. This is accounted for via the size factor, *kb*, which is defined as the ratio of the strength of the part to the strength of the test specimen.

In a search of the literature, the authors found a number of empirical relations for size factor. A number of these are summarized in Table 13-3 of Shigley and Mischke (1986). One that is not tabulated is given by Shigley and Mischke (1989) as follows:

$$kb = (d/0.3)^{-0.1133} \tag{19}$$

where:
kb = Size factor
d = Shaft diameter (inch)

Another relation that the authors have found to be useful is given by Banantine, et al. (1990):

$$kb = 0.869 \bullet d^{-0.097} \tag{20}$$

where:
kb = Size factor
d = Shaft diameter (inch)

Regardless of which method is used to determine it, the authors have found that, similar to the surface finish factor, many engineers erroneously believe that the size factor should be applied to the entire S-N curve. This is refuted by Banantine, et al. (1990), who state that the size effect is observed mainly in the HCF regime. Juvinall (1967) agrees, stating that the effect of part size on static strength and strength at 1000 cycles is much less pronounced than at 10^6 cycles and is commonly neglected.

Accordingly, using the same reasoning as was used for the surface finish factor, the authors advocate using the size factor obtained from the above empirical relations only with the strength for 10^6 cycles. At a life of 1000 cycles, a size factor of unity should be employed, and at all lives between these two points, the size factor versus life characteristic should be assumed to follow a linear relation when plotted on log-log coordinates. The relevant equations are very similar to those previously given for the surface finish factor:

$$kb(N) = 10^b / N^m \tag{21}$$

$$m = \log[kb(1000)/kb(10^6)]/3.0 \tag{22}$$

$$b = \log\{[kb(1000)]^2/kb(10^6)\} \tag{23}$$

where:
kb(N) = Size factor for a life of N cycles
kb(10^6) = Size factor for 10^6 cycles (from Equation (19) or (20))
kb(1000) = Size factor for 1000 cycles (1.00)
m = Slope of kb versus N line on log-log coordinates
b = Intercept of kb versus N line on log-log coordinates

Stress Concentration Factor

The fatigue stress concentration factor, *kf*, is included in Equation (14) since, in the authors' experience and that of Jackson and Umans (1980), almost all torsional vibration fatigue failures occur at locations of geometric stress concentrations such as fillet radii or keyways.

The fatigue stress concentration factor, *kf*, is arrived at by first determining the geometric stress concentration factor, *kt*. This factor is solely dependent on the geometry of the stress raiser and is totally independent of the part's material and condition. Peterson (1974) gives geometric stress concentration factors for virtually any geometry that the user is likely to encounter. Finite element analysis is another effective method for determining values of *kt*.

The geometric stress concentration factor is determined assuming that the part is made from an ideal material that is isotropic, elastic, and homogeneous. Fortunately, the deviations from these assumptions that occur in real materials tend to reduce the impact of the stress raiser. To account for these real effects, a second stress concentration factor, *kf*, which is always less than or equal to *kt*, is defined as follows:

$$kf = 1 + q(kt - 1) \tag{24}$$

where:
kf = Effective stress concentration factor
kt = Geometric stress concentration factor
q = Material notch sensitivity

It is seen that the geometric and effective stress concentration factors are related by a parameter, *q*, which represents how sensitive the material is to notches. The notch sensitivity factor is defined by the above equation and, by definition, is always between zero and one. A material having a notch sensitivity of zero is totally insensitive to notches such that its effective stress concentration factor is always 1.0, regardless of notch geometry. On the other hand, a material having a notch sensitivity of one is extremely sensitive to the presence of notches and, as a result, its geometric and effective stress concentration factors are equal.

In general, the notch sensitivity factor is dependent on the material, its heat treatment, and the size of the notch in question. Juvinall (1967) and Shigley and Mischke (1989) both give plots that can be used to determine the notch sensitivity factor for most practical cases. Once the notch sensitivity is obtained, it should be combined with the geometric stress concentration factor using Equation (24) to obtain the effective stress concentration factor, *kf*.

As was the case with the surface finish and size factors, the effective stress concentration factor determined in the above manner only applies at a life of 10^6 cycles. However, unlike the surface finish and size factors, there is some disagreement over how much the impact of stress concentrations is reduced at a life of 1000 cycles. Shigley and Mischke (1989) recommend that, similar to the cases for surface finish and size factors, the life of 1000 cycles be treated as a static loading case, which has a corresponding *kf* value of 1.0. Evans, et al. (1985), are more conservative, recommending that the square root of the *kf* value corresponding to 10^6 cycles be used at 1000 cycles.

To resolve this discrepancy, the authors turned to Juvinall (1967) who acknowledges that many experts have assumed that the effects of stress raisers are negligible at lives up to 1000 cycles. However, he goes on to say that recent experiments have clearly indicated that this assumption is overly optimistic. Accordingly, the authors have adopted the method of Evans, et al. (1985), by using the following equation:

$$kf(1000) = [kf(10^6)]^{0.5} \tag{25}$$

where:
kf(1000) = Effective stress concentration factor for 1000 cycles
kf (10^6) = Effective stress concentration factor for 10^6 cycles

Once the two endpoints are known, there is nearly unanimous agreement on how *kf* values between 1000 and 10^6 cycles should be determined. Shigley and Mischke (1989), Evans, et al. (1985), and Juvinall (1967) all agree that the *kf* versus *N* characteristic is linear when plotted on log-log coordinates. The reasoning behind this is that doing so keeps the S-N curve linear on log-log coordinates, which agrees with empirical findings. It is this reasoning that was used previously for deciding that the surface finish and size factors should also exhibit the same behavior as a function of life. Parroting the equations previously provided for the surface finish and size factors, the equations for determining *kf* are as follows:

$$kf(N) = 10^b / N^m \tag{26}$$

$$m = \log [kf(1000)/kf(10^6)]/3.0 \tag{27}$$

$$b = \log \{[kf(1000)]^2/kf(10^6)\} \tag{28}$$

where:
kf(N) = Effective stress concentration factor for a life of N cycles
kf(10^6) = Effective stress concentration factor for 10^6 cycles (from Equation (24))
kf(1000) = Effective stress concentration factor for 1000 cycles (from Equation (25))
m = Slope of kf versus N line on log-log coordinates
b = Intercept of kf versus N line on log-log coordinates

It should be noted that the procedure provided herein utilizes the stress concentration factor as a strength reduction factor (per Equation (14)) rather than in the more conventional role of a stress increasing factor. If *kf* were independent of life, the two methods would be equivalent and could be used interchangeably. However, since *kf* is a function of life, it must be used as a strength reduction factor. Thus, the user should remember to not apply a stress concentration factor to the cyclic stress obtained from Equation (7) since stress concentration effects are already accounted for in the S-N curve.

Safety Factor

In a previous paper (Corbo and Malanoski, 1996), the authors reported that an extensive literature search revealed a near unanimous consensus that a safety factor of 2.0 should be employed when comparing calculated and allowable stresses for torsional vibration analyses. However, these recommendations were almost all concerning the safety factor to be applied to the results of a steady-state torsional response analysis. In the authors' experience, the primary reasons why a safety factor is needed for torsional analyses are the inherent uncertainties in the magnitudes of the excitation torques and in the generic damping ratio that is normally applied to each shaft element in the system. However, as Smalley (1983) has noted, the results of a transient response analysis, such as the one under consideration, are much less sensitive to errors in the damping coefficient than are the results of a steady-state response analysis. Furthermore, the magnitudes of the excitation torques in steady-state analyses are usually more uncertain since they are usually based on rules of thumb whereas synchronous motor startup analyses use the actual motor excitation torques. Based on this, the authors have reasoned that a safety factor somewhat lower than the steady-state value of 2.0 would be appropriate for a synchronous motor startup analysis.

Accordingly, the authors sought to determine what transient analysis safety factor would be equivalent to the universally accepted steady-state safety factor of 2.0. In order to do this, the authors made a series of transient and steady-state response runs on a representative synchronous motor driven compressor. For all runs, all parameters were held constant except for the damping ratio, which was systematically varied. Thus, the difference in excitation uncertainties was conservatively ignored and the function of the safety factor was assumed to be solely to account for damping coefficient uncertainties.

The results of these runs are plotted in Figure 6. The abscissa for this plot is the assumed damping ratio while the ordinate is the ratio of the maximum calculated cyclic torque to that obtained using the baseline damping ratio of 2.0 percent. It is easily seen that, as expected, the steady-state runs are far more sensitive to variations in the assumed damping ratio than are the transient runs. Furthermore, it is seen that a 2:1 variation in damping ratio results in a 2:1 change in steady-state response since the response is merely inversely proportional to the damping ratio. However, a 2:1 change in damping ratio results in only about a 30 percent change in the peak torque of the transient analysis. Conservatively assuming that the conventional steady-state safety factor of 2.0 is used to accommodate a 2:1 uncertainty in damping, it is seen that this same uncertainty can be accommodated with a safety factor of about 1.3 for the transient case. For the sake of conservatism, the authors recommend using a safety factor of 1.35 for transient analyses.

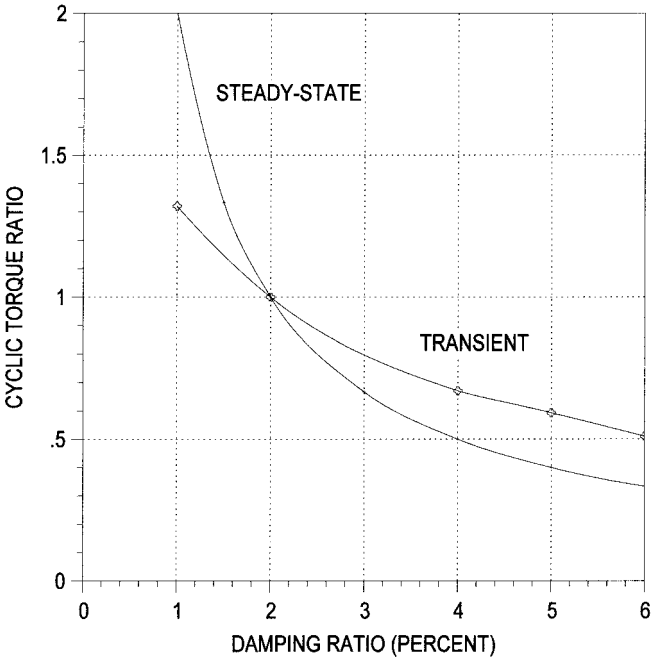

Figure 6. Effects of Varying Damping Ratio.

Once all the derating factors have been determined, the allowable shear stress versus number of cycles curve can be obtained from Equation (14). For each life of interest, Equations (16), (21), and (26) should be used to calculate the surface finish, size, and effective stress concentration factors. These should then be combined with the S-N curve obtained by multiplying Equation (11) by the elastic modulus, the shear factor of 0.577, and the safety factor of 1.35 to determine the allowable shear stress for that life. A series of these calculations can then be used to generate the τ-N curve.

Cumulative Damage Determination

The preceding text provides a method for determining the allowable number of cycles for a given torsional cyclic stress level calculated via Equation (7). If each startup consisted of a single stress cycle repeated a given number of times, the machine's allowable number of starts could be easily determined. However, since the cyclic torque versus time profile typically looks like that of Figure 4, a shaft element will normally be subjected to a number of different cyclic stress levels during a single startup.

Consequently, the shaft's life must be predicted using some type of cumulative damage algorithm. Accordingly, the authors recommend employment of Miner's linear damage rule, which is described in detail by Miner (1945) and is probably the simplest cumulative damage algorithm in common usage. The basis of Miner's rule is that each individual stress cycle where the stress is above the endurance limit consumes a fraction of the part's total life. The fraction of life lost is given by the following:

$$f_I = n_I / N_I \tag{29}$$

where:
f_I = Fraction of life lost
n_I = Total number of applied cycles of given cyclic stress
N_I = Allowable number of cycles for given cyclic stress

For example, if a shaft is subjected to 1500 starts and each start has one loading cycle having a cyclic stress of 25,000 psi, the number of applied cycles would be 1500. Furthermore, if the τ-N curve generated for this shaft using the procedure previously described revealed that the number of allowable cycles for a stress level of 25,000 psi was 15,000 cycles, then N would be 15,000. The fraction of the part's life consumed by this loading cycle would then be 10 percent (1500/15,000).

Theoretically, the part should fail when the summation of the individual life fractions obtained from the above equation equals unity. However, many experimenters have found that the sum at which parts actually fail can vary somewhat from this value. Juvinall (1967) tells of tests in which the summation at failure varied from 0.61 to 2.20. Shigley and Mischke (1989) disagree slightly, claiming that the observed range is from 0.70 to 2.20. Based on these findings and their own experience, the authors have adopted a value of 0.50 as a safe limit for synchronous motor startups. Thus, a part is assumed to fail when:

$$\Sigma (n_I / N_I) = 0.50 \tag{30}$$

Using this rule, the number of starts that a shaft can be safely subjected to can be directly calculated. First, the allowable number of cycles, N_I, for each cyclic stress above the endurance limit that the shaft is subjected to should be determined from the τ-N curve. Then for an assumed number of starts, the number of applied cycles for each cyclic stress, n_I, should be calculated. The fractional damages can then be calculated from Equation (29) and the sum of the fractions can be compared to 0.50. The number of starts that gives a sum of exactly 0.50 is the allowable number of starts.

The authors are fully confident in the use of this procedure even though they are fully aware that some experts such as Manson, et al. (1965), correctly criticize Miner's rule for its failure to account for the order that the stresses are applied in. It is well known that if a part is subjected to its peak stress cycle first and then subjected to progressively decreasing stress cycles, it will fail much quicker than if the stresses are applied in a random order. Under these circumstances, use of Miner's rule will over-predict the part's life. Juvinall (1967) asserts that parts have been observed to fail at a summation of as low as 0.18 when the stresses were applied in this manner.

On the other hand, if the stress cycles are sequentially increased with the peak stress cycle being the last one applied, the life of a part can be dramatically increased. In fact, many investigators have observed that this phenomenon, known as coaxing, results in an increase in the material's endurance limit above its virgin value. For these conditions, Miner's rule under-predicts life, sometimes dramatically. Juvinall (1967) has observed parts that have lasted all the way up to a sum of 23.0 when loaded in this manner.

Fortunately, in synchronous motor startups, the loading is not even close to either of these two extremes. It is the authors' experience that in most synchronous motor startups, the peak stress cycle is chronologically near the middle of the high-stress cycle range such that the number of high-stress cycles occurring before it is about equal to the number after it. This is illustrated in Figure

4. Thus, for this case, the shortcomings of Miner's method are felt to be inconsequential. This conclusion is backed up by Evans, et al. (1985), Wachel and Szenasi (1993), Anwar and Colsher (1979), Joyce, et al. (1978), and Jackson and Umans (1980), all of whom recommend using Miner's rule in the evaluation of synchronous motor startups.

The number of stress cycles that must be included in the Miner's summation varies with the application. As a rule of thumb, Sohre (1965) states that a typical startup involves from 10 to 20 high-stress cycles. The authors' experience is in general agreement with this, although they have seen startups having as few as seven such cycles. The exact number of cycles that have to be considered in the Miner's summation is determined by converting the minimum and maximum torque values into cyclic stresses via Equations (6) and (7). These cyclic stresses should then be compared to the shear endurance limit obtained from Equation (14) since the only cycles that contribute to fatigue damage are those where the cyclic stress exceeds the endurance limit. All such cycles need to be included in the Miner's summation. All other cycles can be discarded.

OTHER STRUCTURAL CONSIDERATIONS

In addition to the ability of the shafts to withstand the required number of starts, several other structural issues must be looked at when evaluating the results of a synchronous motor startup analysis. The peak torques occurring in specialty components such as gears, splines, and couplings should be compared to the component's maximum torque rating to prevent overloading. The peak torques occurring at interference fits retaining impellers or coupling hubs should also be checked to verify that they are not large enough to cause relative motion to occur.

In stark contrast to the steady-state situation, torque reversals occurring at components, such as gears, splines, or couplings, that contain backlash are not a concern in the transient case. Under normal circumstances, these components are continuously loaded in one direction and the system operates totally unaware of the backlash. However, if the magnitude of the induced vibratory torque exceeds the average transmitted torque, the net torque becomes instantaneously negative and a torque reversal is said to have occurred. Whereas this condition can be disastrous in the steady-state, Szenasi and von Nimitz (1978) and Grgic, et al. (1992), note that transient torque reversals are quite common and are normally allowed for in the design of gears and geared couplings.

MODIFICATIONS TO ALLEVIATE PROBLEMS

If the results of the startup analysis meet all the structural criteria given above, the analysis is finished and the machine can be sanctioned. However, in the event that the original design is found wanting, some methods of rectification are as follows:

- *Alter the starting procedure to start the compressor in the unloaded condition*—If the motor must start the compressor in the loaded condition, the compressor load torque is usually quite high. Accordingly, the system's acceleration rate is relatively slow and the dwell time at resonance is, thereby, relatively long. Starting the compressor in the partially or fully unloaded condition will normally speed up the acceleration significantly and reduce the dwell time at resonance. This results in a reduction in peak torque due to insufficient time for it to build up to its previous value as well as a reduction in the number of damaging cycles per startup.

- *Reduce the inertia of the load*—Many authors have noted that synchronous motor startups are more likely to generate problems as the ratio of the load inertia to that of the motor increases. This is probably due to an increased dwell time at resonance, similar to the situation described above.

- *Reduce the motor voltage during starting*—Since the magnitudes of the motor's pulsating torques are approximately proportional to the square of motor voltage, this can result in a significant reduction in the system's peak torques and stresses. The downside of doing this is that it also reduces the motor's average torque, causing the startup to take longer and increasing the dwell time at resonance. However, in the authors' experience, the benefits usually outweigh the drawbacks and many practical machines are started at between 70 and 90 percent of full voltage.

- *Change the motor shaft's coupling to a special damping coupling*—The authors are familiar with many synchronous motor-driven turbomachines that are equipped with a Holset-style coupling on the motor shaft. These couplings contain an elastomeric element that tends to damp out (via material hysteresis) the pulsations generated in the motor. Additionally, placement of this coupling on the motor shaft tends to isolate the excitation source (motor) from the areas where trouble is frequently encountered (gearbox and compressor).

- *Make changes to increase the fundamental frequency*—As was stated previously, most synchronous motor startup problems involve resonance with the fundamental frequency. It is the experience of the authors, and many other experts, that the lower this natural frequency is, the more likely the machine will encounter problems. The explanation for this is twofold. First, as is seen from Figure 2, the lower the fundamental frequency is, the higher its resonant speed will be. Since most motors' pulsating torques increase significantly as synchronous speed is approached, high resonant speeds usually mean large excitations. Second, synchronous motor average torques tend to decrease near synchronous speed such that the machine's acceleration rate tends to be relatively slow as synchronism is approached. Accordingly, resonance dwell times are increased. Thus, any changes that can be made (usually implemented at the motor coupling) to increase the fundamental frequency are usually beneficial.

- *Polish or shot-peen any troublesome shafts*—The beneficial effects that employing a finer surface finish have on fatigue life have already been discussed. However, shot-peening critical shaft surfaces can also result in significantly increased fatigue strengths, sometimes by as much as 30 to 40 percent. The reason for this improvement is that shot-peening leaves the surface in a state of residual compression. Since fatigue failures can only occur if tensile stresses are present, the residual compression must be overcome before the surface stress can become tensile.

- *Alter the motor design so that the crossover point occurs close to resonance*—As is depicted in Figure 1, many synchronous motors have a point somewhere in their speed range where the direct and quadrature axis torques are equal (crossover point). Since the pulsating torque is equal to the difference in these two torques, it is zero at this point. Accordingly, if the motor design can be altered such that the crossover point occurs in the vicinity of resonance, the potential for problems is greatly reduced.

- *Alter the motor and/or system to increase the acceleration at resonance*—Since both the motor's average torque and the compressor's load torque are highly nonlinear as a function of speed, the net torque available to accelerate the machine tends to vary as a function of speed. The net acceleration torque can, thus, be plotted as a function of speed and changes enacted to locate the problem resonant point at a point where the acceleration torque is high to minimize the dwell time at resonance.

- *Change the motor from a solid pole to a laminated rotor design*—In general, laminated rotors tend to generate lower pulsating torques than do solid pole designs and, thus, are less likely to generate problems. However, implementing this change can introduce other problems. Since laminated pole synchronous motors often have average torque versus speed curves that contain large positive slopes, a negative damping effect that can trigger instability problems can result. Additionally, laminated pole motors tend to be more expensive.

If any modifications are implemented, a new system has been created. Accordingly, the entire torsional analysis procedure must be repeated to verify that the change has not introduced any new problems.

OVERALL ANALYSIS PROCEDURE

All the steps of the analysis procedure have been described in detail. To recap, a chronological listing of the steps to be taken is as follows:

1. Generate lumped parameter model.
2. Determine undamped natural frequencies and mode shapes.
3. Verify undamped analysis results using hand calculations.
4. Generate Campbell diagrams.
5. Reduce lumped parameter model in preparation for transient analysis (if necessary).
6. Verify that first two natural frequencies of reduced model are same as for original model.
7. Run synchronous motor startup analysis
   - Input motor average and pulsating torques and load torques as functions of speed.
   - Select appropriate damping ratio to apply to all shafts in model.
   - Select time step to avoid numerical instabilities.
   - Obtain torque versus time histories for all shaft elements.
8. Select shaft elements to run fatigue calculations on.
   - Shafts having small diameters
   - Shafts having significant stress concentrations
   - Any shaft containing a keyway
9. For each shaft of interest, determine the strain-life curve from Equation (11).
10. Generate the baseline tensile stress versus life curve by multiplying the strain-life curve by the elastic modulus.
11. Determine the geometric stress concentration factor, *kt*, from the shaft's geometry.
12. Determine the notch sensitivity factor, *q*.
13. Determine the effective stress concentration factor, *kf*, for 10^6 cycles from Equation (24).
14. Determine the surface finish factor, *ka*, for 10^6 cycles.
15. Determine the size factor, *kb*, for 10^6 cycles.
16. Using Equations (16), (21), and (26), calculate *kf*, *ka*, and *kb* as functions of life, *N*.
17. Using a shear factor of 0.577, a safety factor of 1.35, and Equation (14), determine τ-N curve.
18. Using Equations (6) and (7), calculate cyclic shear stress, τ_{cyclic}, for each high-stress cycle.
19. Use τ-N curve to find allowable number of cycles, *N*, for each value of cyclic shear stress.
20. Determine number of starts that makes Equation (30) true. This is the allowable number of starts.
21. Check for any other structural problems.
22. If necessary, implement modifications to alleviate structural problems.
23. Repeat above procedure for new system resulting from step 22 changes.

EXAMPLE ILLUSTRATING PROCEDURE

The presented procedure is best illustrated by an example. The authors recently completed the design of a 66,000 hp air compression unit. The centrifugal compressor, which runs at 4298 rpm, is driven by a synchronous motor operating at 1800 rpm through a one-stage step-up gearbox. Both the high- and low-speed shafts contain flexible diaphragm couplings.

Per the advocated procedure, a lumped parameter model was constructed for the entire drive train and undamped analysis was run on it. The first two natural frequencies, whose mode shapes are presented in Figures 7 and 8, were found to occur at 14.0 and 34.0 Hz. A Campbell diagram (not shown) was then generated to account for the system's steady-state excitations and no steady-state resonance points were found. The motor shaft Campbell diagram of Figure 9 was then generated to determine the potential resonances triggered by the synchronous motor excitation.

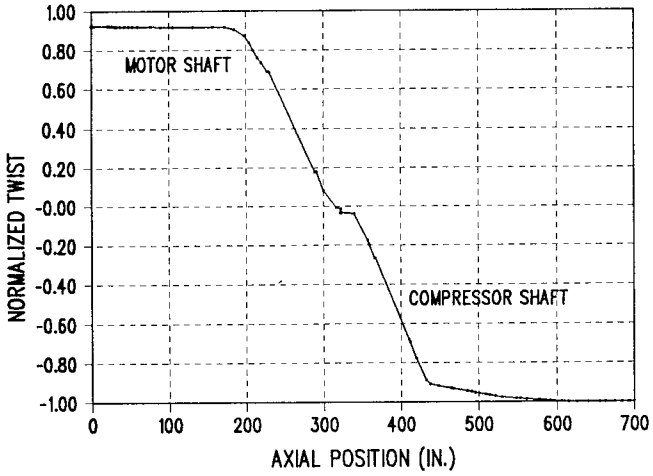

Figure 7. Air Compressor First Mode Shape.

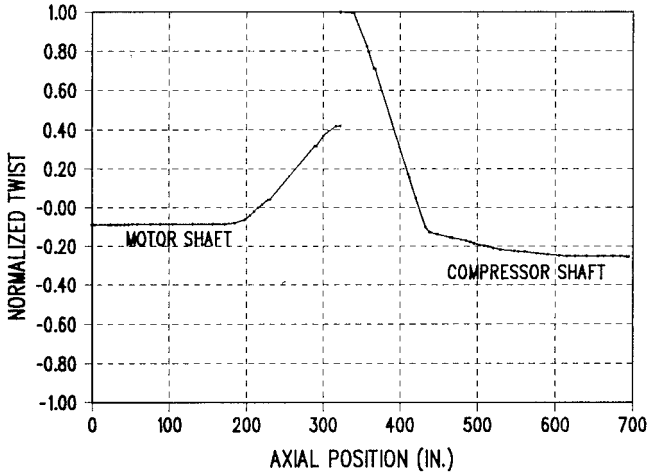

Figure 8. Air Compressor Second Mode Shape.

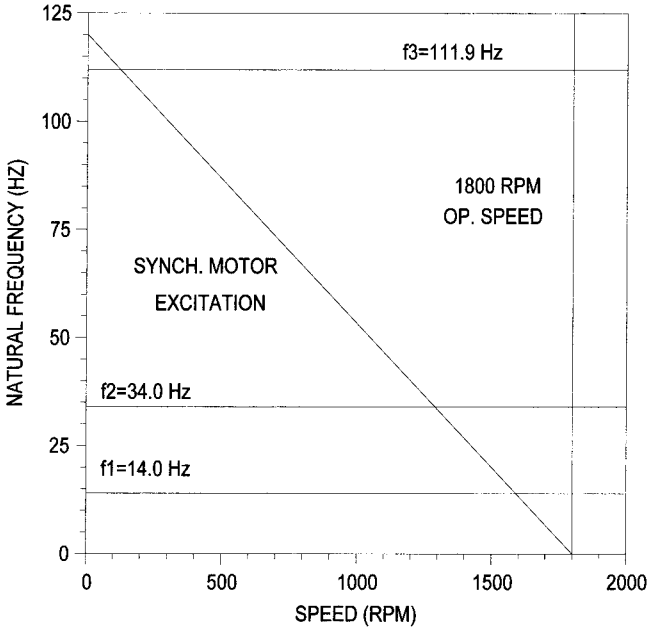

Figure 9. Air Compressor Campbell Diagram.

It is seen from the figure that the synchronous motor excitations create three resonance points—with the first, second, and third natural frequencies. Per the authors' experience, the resonance with the third natural frequency was ignored since that frequency seldom participates in synchronous motor responses, especially when its resonance point is at such a low speed. Thus, the transient response analysis focused on simulating the responses at the first two natural frequencies with the fundamental being the primary concern since its resonance point occurs at such a high speed (1590 rpm or 88 percent of synchronous speed).

To accommodate the limitations of the transient response analysis program employed, the original model, which contained 74 stations, was reduced to an equivalent five-disk model. Each shaft element in the model represented one of the primary shafts in the drive train—motor shaft, gearshaft, pinion shaft, and compressor shaft. Undamped analysis was then performed on the reduced model and the first two natural frequencies were verified to still be at 14.0 and 34.0 Hz.

Once the reduced model was validated, the transient analysis was run. Since the undamped analysis revealed that the reduced model's highest (fourth) natural frequency occurred at 115.3 Hz, its corresponding period was 0.0087 seconds. In accordance with the guidelines provided previously, a generic damping ratio of two percent of the critical value and a time step of 0.001 seconds were employed. Gear backlash effects were ignored.

The results of the transient analysis consisted of the time histories of the torque in all four shafts. These plots revealed that the response as the system passed through the second natural frequency resonance point was inconsequential. However, as expected, a significant resonance was observed at a motor speed of about 1608 rpm, representing excitation of the fundamental frequency at 14.0 Hz.

The response in the resonance region for the motor shaft is presented in Figure 10. It should be noted that the torque plotted as the ordinate is expressed in the peculiar units of "per unit" (pu). This is a shorthand method of expressing the ratio of the actual torque to the motor's rated torque at synchronous speed. For this motor, one pu is equal to 2.31E6 in-lb.

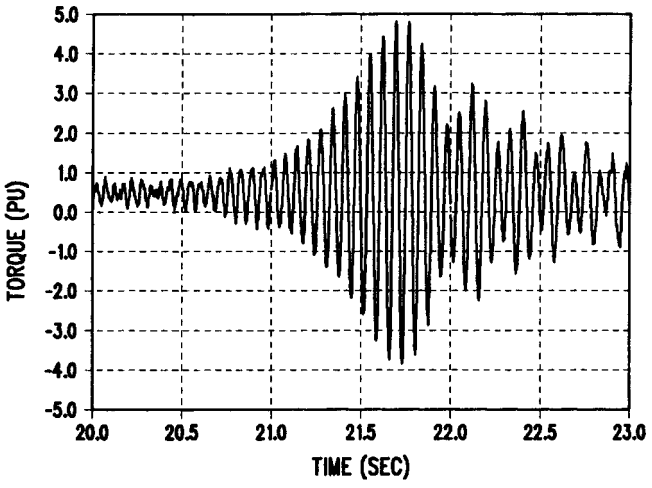

Figure 10. Air Compressor Calculated Response.

Examination of the figure reveals that the torque is fairly smooth up until resonance is approached. In this region, the mean torque is seen to be positive, representing the torque required to drive the load. The relatively small ripple that is superimposed on the mean torque represents the relatively small response to the synchronous motor's pulsations.

Once the resonance zone is entered at about 21.2 seconds, the ripple rises steadily until it reaches a peak at about 21.75 seconds. At this peak, the maximum torque is seen to be almost 5.0 pu while the minimum is almost −4.0 pu. Referral to the speed versus time plot (not shown) revealed the speed at this peak to be about 1608 rpm, confirming that the unit is in resonance with its first natural frequency. The peak torque is followed by several more high torque cycles of progressively smaller amplitudes until the torque once again levels off as the resonance zone is exited.

Although all four shafts had similar response profiles and were analyzed to determine how many starts they could take, this discussion will only consider the motor shaft. The first decision that needed to be made was which portion of the shaft represented the "weak link." Although this decision is not always straightforward, in this case it was since the shaft's smallest diameter also contained a significant stress concentration. The shaft diameter at that location was 13.17 inches.

Attention then turned to generating the allowable shear stress versus number of cycles curve for this shaft. The shaft material was 4340 stainless steel, which had an ultimate strength of 120,000 psi and a reduction in area of 40 percent. Accordingly, using Equations (12) and (13), the Coffin-Manson coefficients were calculated to be 200,000 psi ($\sigma_f`$) and 0.5108 ($\varepsilon_f`$). Using these values with empirically-determined proprietary values for the exponents, *b* and *c*, in Equation (11), the strain-life curve was generated. Multiplying all strain values by the elastic modulus of 28.5 million psi then yielded the tensile stress versus life curve for the polished test specimen.

Using the plot for a filleted shaft under torsional loading found in Peterson (1974), the geometric stress concentration factor, *kt*, was estimated to be 1.55. Using Juvinall (1967), the notch sensitivity, *q*, was then determined to be 0.91. Substituting these values into Equation (24), the effective stress concentration factor, *kf*, for a life of 10^6 cycles was found to be 1.501.

Using Equation (15), the 10^6 cycle surface finish factor was calculated to be 0.90 for the ground surface. Determination of the size factor was not as simple as merely using Equation (19) or (20) since our shaft's diameter was so large that it was outside the size range that the providers of those relations claimed they were valid for. Accordingly, proprietary test data were utilized to come up with a size factor of 0.667 for a life of 10^6 cycles. It should be noted that the predictions of Equations (19) and (20), 0.651 and 0.677, respectively, are close enough to the empirically derived value that the authors feel that either of those equations can probably be used in this size range.

Once the values of *ka*, *kb*, and *kf* were obtained for a life of 10^6 cycles, the values at all other lives were determined. Using the equations provided previously, the slopes (*m*) and intercepts (*b*) for these three parameters on log-log coordinates were determined to be:

- Surface finish factor: m = 0.015252, b = 0.045757
- Size factor: m = 0.058625, b = 0.175874
- Stress concentration factor: m = −0.029373, b = 0.0

Using these values in Equations (16), (21), and (26), the variations of the three factors with life were calculated and are presented in Table 1. Then, employing these factors, a shear factor of 0.577 and a safety factor of 1.35, the baseline tensile S-N curve was converted to a τ-N curve using Equation (14). Selected values from this curve are also tabulated in Table 1.

Once the τ-N curve was obtained, the next task was to determine the number of applied stress cycles for each start and the stress levels corresponding to each cycle. There are a number of ways to convert the results of a transient analysis in the form of Figure 10 to a tabulation of stress cycles having minimum and maximum stresses. Jackson and Umans (1980) discuss the peak counting method in which each cycle is merely assumed to have a cyclic torque that is equal to the peak torque obtained from the transient analysis. For instance, the peak torque occurring in Figure 10 is +4.811 pu. Thus, using the peak counting method, the cycle would be assumed to consist of a torque range from −4.811 to +4.811 pu.

Table 1. Air Compressor Allowable Stresses.

ALLOWABLE CYCLES N	K_A	K_B	K_F	ALLOWABLE SHEAR STRESS (PSI)
1000	1.000	1.000	1.225	119,302
2000	0.989	0.960	1.250	83,495
3000	0.983	0.938	1.265	68,725
5000	0.976	0.910	1.284	54,612
7500	0.970	0.889	1.300	46,066
1.0E4	0.965	0.874	1.311	41,092
1.5E4	0.960	0.853	1.326	35,288
2.0E4	0.955	0.839	1.338	31,864
2.5E4	0.952	0.828	1.346	29,534
3.0E4	0.949	0.819	1.354	27,813
4.0E4	0.945	0.806	1.365	25,386
5.0E4	0.942	0.795	1.374	23,716
6.0E4	0.939	0.787	1.381	22,470
7.0E4	0.937	0.780	1.388	21,492
8.0E4	0.935	0.773	1.393	20,696
9.0E4	0.934	0.768	1.398	20,029
1.0E5	0.932	0.763	1.402	19,460
1.5E5	0.926	0.745	1.419	17,479
2.0E5	0.922	0.733	1.431	16,248
3.0E5	0.917	0.716	1.448	14,715
5.0E5	0.910	0.695	1.470	13,059
7.5E5	0.904	0.678	1.488	11,922
1.0E6	0.900	0.667	1.501	11,194

This is obviously over-conservative since the minimum torques displayed in Figure 10 all have magnitudes below 4.0 pu and is not recommended for use.

Jackson and Umans (1980) then proceed to describe a less conservative cycle counting procedure known as the rain-flow method. Although this method is probably the most accurate one available for analyzing profiles where the torque varies randomly, the authors do not believe that its complexity is warranted for the predictable profiles obtained from synchronous motor startups. Instead, the authors have had considerable success using a simple chronological counting procedure. The peak torque is identified and the minimum torques preceding and succeeding the peak torque are then checked. Whichever minimum torque has the greater magnitude is paired with the peak torque and all other torque peaks are then paired in the same manner.

Use of this procedure is illustrated by referral to Figure 10. As stated previously, the peak torque is +4.811 pu. The minimum torque peaks preceding and following this peak are −3.743 and −3.848 pu, respectively. Since the following peak has a larger magnitude, it is selected for pairing with the +4.811 pu peak. Accordingly, the first torque cycle is assumed to be from +4.811 to −3.848 pu. All other cycles are determined by pairing the positive peak with the negative peak immediately following it. The resulting torque cycles obtained from applying this procedure to the profile of Figure 10 are presented in Table 2.

Table 2. Air Compressor Cumulative Damage Assessment.

PEAK NO.	DESCRIPTION	T_{MAX} (PU)	T_{MIN} (PU)	T_{MAX} (IN-LBF)	T_{MIN} (IN-LBF)	τ_{MAX} (PSI)	τ_{MIN} (PSI)	τ_{CYCLIC} (PSI)	APPLIED CYCLES n	ALLOW. CYCLES N	n/N
1	PEAK	4.811	-3.848	1.11134E7	-8.88888E6	24,778	-19,818	22,298	7307	61,608	0.119
2	PEAK + 1	4.802	-3.615	1.10926E7	-8.35065E6	24,731	-18,618	21,675	7307	67,963	0.108
3	PEAK + 2	4.236	-2.867	9.78516E6	-6.62277E6	21,816	-14,766	18,291	7307	125,945	0.058
4	PEAK + 3	3.170	-1.641	7.32270E6	-3.79071E6	16,326	-8,451	12,389	7307	628,026	0.012
5	PEAK - 1	4.434	-3.743	1.02425E7	-8.64633E6	22,836	-19,277	21,057	7307	75,235	0.097
6	PEAK - 2	3.974	-3.249	9.17994E6	-7.50519E6	20,467	-16,733	18,600	7307	118,225	0.062
7	PEAK - 3	3.415	-2.589	7.88865E6	-5.98059E6	17,588	-13,334	15,461	7307	244,197	0.030
8	PEAK - 4	2.959	-2.176	6.83529E6	-5.02656E6	15,239	-11,207	13,223	7307	474,108	0.015

Once the method for determining torque cycles had been decided on, the next order of business was determining how many cycles needed to be considered. In order to determine this, the torque values were converted into cyclic stress values via Equations (6) and (7). These cyclic stresses were then compared to the shear endurance limit, which is seen to be 11,194 psi from Table 1. Thus, all cycles having a calculated cyclic stress of 11,194 psi or greater were retained and the remaining ones were discarded. It is seen from Table 2 that doing this eliminated all but eight stress cycles. In addition to the peak cycle, there are the four cycles immediately preceding it (denoted in the table by N-1, N-2, etc.) and the three cycles immediately following it.

For each of these cycles, the cyclic stress is used with the τ-N curve to determine the allowable number of cycles, *N*. For instance, for the peak cycle, which has a cyclic stress of 22, 298 psi, referral to Table 1 reveals that *N* is somewhere between 6.0E4 and 7.0E4 cycles. Using the actual equation, *N* is computed to be 61,608 (6.16E4) cycles. The allowable number of cycles for all other stress cycles was calculated in exactly the same manner.

The only remaining task is the calculation of the allowable number of starts for this shaft. For this case, which is highly typical of synchronous motor startups, each stress cycle is applied only once per startup. Thus, if the unit were subjected to *n* startups, the applied number of cycles for each tabulated cycle would be *n*. Although *n* can still be determined by trial and error, rearrangement of Equation (30) yields the following explicit relation for *n*:

$$n = 0.5 / \Sigma (1 / N_I) \tag{31}$$

where:
n = Allowable number of starts
N_I = Allowable number of cycles for Ith cycle

Using this equation, the allowable number of starts is calculated to be 7307. When this value is substituted for *n* in Table 2, it is verified that the sum of the expended lives is approximately 0.50, in accordance with Miner's rule. Since this unit was required to demonstrate structural integrity for 5000 starts, this shaft was declared fully satisfactory.

ADVANTAGES OF NEW PROCEDURE OVER TRADITIONAL METHOD

The reader may not yet grasp the significance of the advantages that utilizing the shaft life prediction rules provided herein have over the traditional method. After all, many of the rules, such as assuming that the surface finish factor is variable instead of constant, may appear to merely be small tweaks to the conventional method. However, the log-log nature of the τ-N curve means that small changes in predicted strength translate into large changes in predicted life. This large gain can be appreciated by examination of Table 1. It is seen that the strength for 10^4 cycles is 41,092 psi while that for 10^5 cycles is 19,460 psi. It is, thereby, seen that a 2:1 change in strength corresponds to a 10:1 change in life. Accordingly, use of each of the rules presented herein yields a significant increase in predicted life compared to the conventional method.

To illustrate how powerful these effects are, the authors have run a number of cases for the motor shaft described in the previous example and the results are presented in Table 3. Case A is the one presented in the example using the new procedure. All other cases were run by changing one of the new procedure's rules back to its counterpart in the traditional method. The impact of the rule changes advocated herein can, thereby, be clearly seen.

In case B, the strain-life procedure for determining the τ-N curve was replaced by the traditional stress-life method described previously. It is seen that this change alone results in a reduction in predicted life from 7307 to 2237 starts, a huge reduction. This is consistent with the advantages of using the strain-life theory cited by other authors.

Table 3. Impact of Varying Model Assumptions.

CASE	DESCRIPTION	ALLOWABLE NUMBER OF STARTS	PERCENT CHANGE FROM BASELINE
A	BASELINE - RECOMMENDED PROCEDURE USED	7307	--
B	STRESS LIFE THEORY USED INSTEAD OF STRAIN-LIFE THEORY	2237	-69.4 %
C	K_f ASSUMED CONSTANT AT 10^6 CYCLES VALUE	5562	-23.9 %
D	K_a ASSUMED CONSTANT AT 10^6 CYCLES VALUE	6382	-12.7 %
E	K_b ASSUMED CONSTANT AT 10^6 CYCLES VALUE	4011	-45.1 %
F	MAX SHEAR STRESS THEORY USED INSTEAD OF VON MISES	4346	-40.5 %
G	SAFETY FACTOR CHANGED TO 2.0	1940	-73.5 %
H	ALL ABOVE CHANGES APPLIED TOGETHER	56	-99.2 %

In cases C, D, and E, the traditional method of applying the 10^6 cycle values of *kf*, *ka*, and *kb* to the entire S-N curve are employed. It is seen that all these changes have significant impact, especially that involving the size factor, *kb*. This large effect is due to the large diameter shaft being studied and should not be as dramatic for more conventional shaft sizes.

In case F, the method of calculating the shear strength from the known tensile strengths has been changed from the maximum shear stress theory to the distortion energy (von Mises) theory. Although the two theories do not appear to differ that much (.500 versus .577 factor), the impact of the change is seen to be substantial.

In case G, the stress safety factor has been changed from the recommended value of 1.35 to the traditional value of 2.00. The change in predicted life is amazingly high, suggesting that the large majority of organizations performing torsional analyses are conservative.

Finally, in case H, all the traditional rules are used together. It is seen that doing this reduces the predicted number of starts from 7307 to a mere 56. Thus, the traditional method predicts that a perfectly good shaft has virtually no startup capability whatsoever. The authors hope that the advantages of using the new procedure are now making themselves apparent to the reader.

CONCLUSION

A comprehensive procedure for the analysis of torsional vibration in turbomachines being driven by synchronous motors has been presented. The methodology is general enough that it should be applicable to any synchronous motor-driven turbomachine. The key points that should be emphasized are as follows:

- A thorough torsional vibration analysis should always be included as an integral part of the design process for *any* turbomachine.
- Turbomachines driven by synchronous motors need to be handled with extra caution due to the large pulsating torques they generate during starting.
- The traditional method for calculating shaft fatigue lives (stress-life method) is over-conservative. The strain-life theory provides a much better calculation tool.
- There is currently a tremendous amount of confusion regarding the proper manner in which fatigue strength reduction factors should be applied. The method presented herein attempts to resolve that confusion.
- The traditional torsional vibration stress safety factor of 2.0, while being perfectly appropriate for steady-state situations, is too conservative for transient analyses.
- Because of the log-log nature of the strength versus life curve, small errors in calculated strengths can lead to large errors in life prediction.
- Torsional vibration and fatigue life analysis are not exact sciences that can be performed by just anybody. The importance of the skill, judgment, and experience of the analyst should never be underestimated.

REFERENCES

Anwar, I. and Colsher, R., 1979, "Computerized Time Transient Torsional Analysis of Power Trains," ASME Paper 79-DET-74.

Banantine, J. A., Comer, J. J., and Handrock, J. L., 1990, *Fundamentals of Metal Fatigue Analysis*, Englewood Cliffs, New Jersey: Prentice Hall.

Bogacz, R., Irretier, H., and Szolc, T., 1990, "Analysis of Transient Torsional Vibrations in the Rotor Machine Using a Hybrid Model," *Proceedings of the Third International Conference on Rotordynamics*, IFToMM, Lyon, France, pp. 207-211.

Boyer, H., 1986, *Atlas of Fatigue Curves*, ASTM.

Chen, H. M., McLaughlin, D. W., and Malanoski, S. B., 1983, "A Generalized and Simplified Transient Torque Analysis for Synchronous Motor Drive Trains," *Proceedings of the Twelfth Turbomachinery Symposium*, Turbomachinery Laboratory, Texas A&M University, College Station, Texas, pp. 115-119.

Chen, W. J., 1995, "Torsional Vibrations of Synchronous Motor Driven Trains Using P-Method," ASME Journal of Vibration and Acoustics, pp. 152-160.

Corbo, M. A. and Malanoski, S. B., 1996, "Practical Design Against Torsional Vibration," *Proceedings of the Twenty-Fifth Turbomachinery Symposium*, Turbomachinery Laboratory, Texas A&M University, College Station, Texas, pp. 189-222.

Draminsky, P., 1948, "Crankshaft Damping," Proceedings of the Institution of Mechanical Engineers, pp. 416-432.

Evans, B. F., Smalley, A. J., and Simmons, H. R., 1985, "Startup of Synchronous Motor Drive Trains: The Application of Transient Torsional Analysis to Cumulative Fatigue Assessment," ASME Paper 85-DET-122.

Grgic, A., Heil, W., and Prenner, H., 1992, "Large Converter-Fed Adjustable Speed AC Drives for Turbomachines," *Proceedings of the Twenty-First Turbomachinery Symposium*, Turbomachinery Laboratory, Texas A&M University, College Station, Texas, pp. 103-112.

Jackson, M. C. and Umans, S. D., 1980, "Turbine–Generator Shaft Torques and Fatigue: Part III—Refinements to Fatigue Model and Test Results," IEEE Transactions on Power Apparatus and Systems, pp. 1259-1268.

Joyce, J. S., Kulig, T., and Lambrecht, D., 1978, "Torsional Fatigue of Turbine Generator Shafts Caused by Different Electrical System Faults and Switching Operations," IEEE PES Winter Meeting, New York, New York.

Juvinall, R., 1967, *Engineering Considerations of Stress, Strain, and Strength*, New York, New York: McGraw-Hill, Inc.

Manson, S. S., Nachtigall, A. J., Ensign, C. R., and Freche, J. C., 1965, "Further Investigation of a Relation for Cumulative Fatigue Damage in Bending," ASME Journal of Engineering for Industry, pp. 25-35.

Miner, M. A., 1945, "Cumulative Damage in Fatigue," ASME Journal of Applied Mechanics, pp. A159-A164.

Mischke, C. R., 1982, "Predicting Fatigue Endurance Strengths for High- and Low-Cycle Fatigue," ASME Journal of Mechanical Design, pp. 653-660.

Mruk, G., Halloran, J., and Kolodziej, R., 1978, "New Method Predicts Startup Torque—Part 1: Analytical Model," *Hydrocarbon Processing*, pp. 181-186.

Peterson, R. E., 1974, *Stress Concentration Factors*, New York, New York: John Wiley and Sons.

Pollard, E. I., 1980, "Synchronous Motors … Avoid Torsional Vibration Problems," *Hydrocarbon Processing*.

Shannon, J. F., 1935, "Damping Influences in Torsional Oscillation," Proceedings of the Institution of Mechanical Engineers, pp. 387-435.

Shigley, J. E. and Mischke, C. R., 1986, *Standard Handbook of Machine Design*, New York, New York: McGraw-Hill, Inc.

Shigley, J. E. and Mischke, C. R., 1989, *Mechanical Engineering Design*, Fifth Edition, New York, New York: McGraw-Hill, Inc.

Simmons, H. R. and Smalley, A. J., 1984, "Lateral Gear Shaft Dynamics Control Torsional Stresses in Turbine-Driven Compressor Train," ASME Journal of Engineering for Gas Turbines and Power, pp. 946-951.

Smalley, A. J., 1983, "Torsional System Damping," *Proceedings of the Seventh Annual Meeting of the Vibration Institute*, The Vibration Institute, Houston, Texas.

Sohre, J. S., 1965, "Transient Torsional Criticals of Synchronous Motor Driven, High-Speed Compressor Units," ASME Paper 65-FE-22.

Szenasi, F. R. and von Nimitz, W. W., 1978, "Transient Analyses of Synchronous Motor Trains," *Proceedings of the Seventh Turbomachinery Symposium*, Turbomachinery Laboratory, Texas A&M University, College Station, Texas, pp. 111-117.

Wachel, J. C. and Szenasi, F. R., 1993, "Analysis of Torsional Vibrations in Rotating Machinery," *Proceedings of the Twenty-Second Turbomachinery Symposium*, Turbomachinery Laboratory, Texas A&M University, College Station, Texas, pp. 127-151.

Walker, D. N., Adams, S. L., and Placek, R. J., 1981, "Torsional Vibration and Fatigue of Turbine-Generator Shafts," IEEE Transactions on Power Apparatus and Systems, pp. 4373-4380.

Wright, J., 1975, "Large Synchronous Motor Drives: A Review of the Torsional Vibration Problem and Its Solution," Koppers Company, Inc., Baltimore, Maryland.

BIBLIOGRAPHY

Artilles, A., Smalley, A. J., and Lewis, P., 1975, "Mill Drive System Vibrations," Proceedings of the National Conference on Power Transmission, Chicago, Illinois.

Brown, R. N., 1960, "A Torsional Vibration Problem as Associated with Synchronous Motor Driven Machines," ASME Journal of Engineering for Power, pp. 215-220.

De Choudhury, P., 1986, "Torsional System Design Relative to Synchronous Motor Start-Up with a Variable Frequency Power Supply System," *Proceedings of the Second International Conference on Rotordynamics*, IFToMM, Tokyo, Japan, pp. 325-328.

Ehrich, F. F., 1992, *Handbook of Rotordynamics*, New York, New York: McGraw-Hill, Inc.

Eshleman, R. L., 1977, "Torsional Vibration of Machine Systems," *Proceedings of the Sixth Turbomachinery Symposium*, Turbomachinery Laboratory, Texas A&M University, College Station, Texas, pp. 13-22.

Grover, H., 1954, *The Fatigue of Metals and Structures*.

Iwatsubo, T., Yamamoto, Y., and Kawai, R., 1986, "Startup Torsional Vibration of Rotating Machine Driven by Synchronous Motor," *Proceedings of the Second International Conference on Rotordynamics*, IFToMM, Tokyo, Japan, pp. 319-324.

Jackson, M. C., Umans, S. D., Dunlop, R. D., Horowitz, S. H., and Parikh, A. C., 1979, "Turbine-Generator Shaft Torques and Fatigue: Part I—Simulation Methods and Fatigue Analysis," IEEE Transactions on Power Apparatus and Systems, pp. 2299-2307.

Ker Wilson, W., 1956, *Practical Solution of Torsional Vibration Problems*, Volumes 1, 2, and 3, New York, New York: John Wiley and Sons.

Manson, S. S., Nachtigall, A. J., and Freche, J. C., 1961, "A Proposed New Relation for Cumulative Fatigue Damage in Bending," ASTM Proceedings, pp. 679-703.

Manson, S. S., 1966, "Interfaces Between Fatigue, Creep, and Fracture," Lewis Research Center, Cleveland, Ohio.

Mruk, G. K., 1978, "Compressor Response to Synchronous Motor Startup," *Proceedings of the Seventh Turbomachinery Symposium*, Turbomachinery Laboratory, Texas A&M University, College Station, Texas, pp. 95-101.

Nelson, D. V. and Sheppard, S. D., 1995, "Fatigue and Fracture Estimation for Metallic Components: Some Current Methods and Future Developments," ASME Journal of Mechanical Design, pp. 121-127.

Nestorides, E., 1958, *A Handbook on Torsional Vibration*, London, England: Cambridge University Press.

Pollard, E. I., 1967, "Torsional Response of Systems," ASME Journal of Engineering for Power, pp. 316-324.

Smalley, A. J., 1974, "Transient Torsional Vibration," Mechanical Technology Incorporated, Latham, New York.

Thames, P. B. and Heard, T. C., 1959, "Torsional Vibrations in Synchronous Motor-Geared-Compressor Drives," AIEE Transactions, pp. 1053-1056.

Vance, J. M., 1988, *Rotordynamics of Turbomachinery*, Chapter 3, New York, New York: John Wiley and Sons.

Williams, P. N., McQuin, N. P., and Buckland, J. E., 1989, "The Importance of Complete Drive Train Analysis for Brushless Salient Pole Motor Drives," *Proceedings of the Fourth International Conference on Electrical Machines and Drives*, IEE-England, pp. 210-214.

ACKNOWLEDGEMENTS

The authors would like to recognize the contributions of Stan Malanoski of No Bull Engineering, Urs Baumann of Sulzer Turbo, John Cimusz of Star Enterprises, Mark DeBlock of General Electric, and Stan Polonski of Praxair who all provided valuable suggestions and feedback during the development of the analysis procedure presented herein.